Enhanced Thermo-Mechanical Decoupling Using Fiber Bragg Grating Sensors in Birefringent Fibers for Structural Health Monitoring

CASCIARO EMANUELE, HENRIQUET DIEGO
and BETTINI PAOLO

ABSTRACT

Fiber optic sensors are increasingly used in aerospace applications due to their lightweight, immunity to electromagnetic interference and ability to measure multiple parameters like strain and temperature. Fiber Bragg Grating (FBG) sensors are particularly promising for Structural Health Monitoring (SHM) but face challenges in distinguishing thermal and mechanical effects, as both induce similar wavelength shifts. Current decoupling methods are classified as extrinsic (requiring additional components) or intrinsic (leveraging sensor properties). While extrinsic methods are effective, they increase system complexity. Intrinsic approaches reduce invasiveness but remain underdeveloped for practical applications. This study introduces birefringent optical fibers with inscribed FBG sensors to address these limitations. Birefringence, caused by refractive index asymmetry, generates two distinct reflection peaks with different sensitivities to strain and temperature, enabling effective decoupling. Experimental validation confirmed the method's accuracy and repeatability. To enhance performance, an optimized resolution strategy was developed, improving measurement accuracy and reducing errors. Machine learning techniques were also explored to refine data analysis. Results demonstrate that birefringent FBG sensors offer a scalable, non-invasive solution for aerospace SHM. Future research will focus on optimizing sensor integration and performance, with an emphasis on collaboration with industry to enable real-world applications.

INTRODUCTION

In recent years, the increasing complexity and safety-critical nature of aeronautical structures have driven the development of advanced SHM strategies. In the aerospace sector, where rigorous and frequent inspections are mandated, integrated SHM systems represent a key technological opportunity.

Casciaro Emanuele, PhD Student, Email: emanuele.casciaro@polimi.it. Department of Aerospace Science and Technology (DAER), Politecnico di Milano, Milan, Italy.
Henriquet Diego, Master Student, Email: diego.henriquet@mail.polimi.it. Master's degree student, Politecnico di Milano, Milan, Italy.
Bettini Paolo, Associate Professor, Email: paolo.bettini@polimi.it. Department of Aerospace Science and Technology (DAER), Politecnico di Milano, Milan, Italy.

Among the technologies for SHM, FBGs are gaining increasing attention due to their high sensitivity, durability and ability to be integrated within composite structures. Despite their numerous advantages, the simultaneous sensitivity to both mechanical strain and temperature presents a major limitation. A single FBG sensor cannot inherently distinguish between mechanical and thermal effects. This challenge has prompted the development of various strategies aimed at decoupling these contributions.

The capillary method, for instance, employs two spatially proximate FBGs, with one isolated in a capillary tube to render it exclusively sensitive to temperature [1]. Alternative approaches include the use of hybrid sensors [2], multi-mode fiber gratings [3] and combinations of FBGs with long-period gratings (LPGs) [4]. However, these methods suffer from mechanical fragility and implementation complexity. Consequently, most of them remain confined to laboratory-scale investigations.

An alternative solution involves the use of polarization-maintaining (PM) optical fibers, which are inherently birefringent and can provide two wavelengths from a single sensing element. This enables local decoupling of thermal and mechanical effects in a robust and compact format [5]. Previous studies [6, 7] have validated the feasibility of this system to achieve effective decoupling. Notably, an analytical method was proposed that utilizes the wavelength associated with the fast polarization axis and the spectral separation between the fast and slow peaks. The efficiency of thermo-mechanical decoupling was assessed using the parameter E_d, a metric introduced in [4] that quantifies the degree of decoupling, ranging from 0 to 1 (ideal decoupling). Considering a generic system of equations with determinant D, it is possible to compute the parameter E_d.

$$\begin{bmatrix} S_1 \\ S_2 \end{bmatrix} = \begin{bmatrix} a & b \\ c & d \end{bmatrix} \begin{bmatrix} T \\ \epsilon \end{bmatrix} \tag{1}$$

$$E_d = \frac{|D|}{\sqrt{(a^2 + c^2)(b^2 + d^2)}} \,. \tag{2}$$

A comparison was carried out among different strategies, considering the condition number K and E_d: tracking fast and slow peaks (Case 1), tracking the slow peak and the peaks difference (Case 2), tracking the fast peak and the peaks difference (Case 3).

The residuals distribution between measured and estimated strain and temperature for Case 3 are $-1.65 \pm 3.1\,^{\circ}C$ and $58.28 \pm 56.2\,\mu\epsilon$. This strategy was deemed superior due to its lower condition number and enhanced sensitivity to strain.

Despite the improvements, high condition numbers remain a concern due to the risk of numerical instabilities. Therefore, this study explores both analytical methods and supervised machine learning (ML) algorithms to further enhance system robustness and accuracy. The developed method successfully decouples thermal and mechanical effects.

TABLE I. Determinant, E_d and condition number K for Case 1 (fast peak and slow peak), Case 2 (slow peak and peak difference) and Case 3 (fast peak and peak difference).

	$D\,[nm^2/^{\circ}C\epsilon]$	$E_d\,[\%]$	K
Case 1	0.9854	4.06	2338835
Case 2	0.9854	8.32	1188266
Case 3	0.9854	7.92	1151158

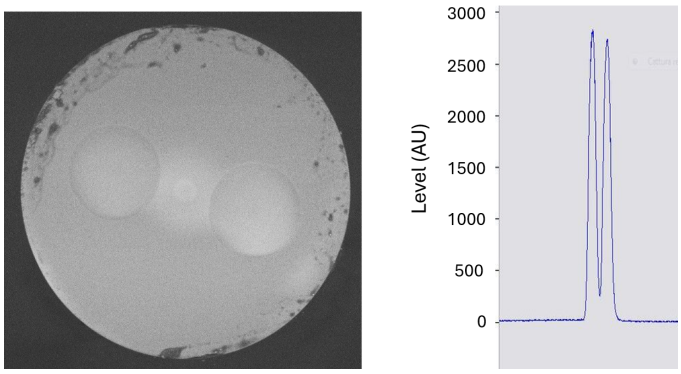

Figure 1. (left) Cross-section of polarization-maintaining PANDA fiber. (right) Reflected spectrum from FBG sensor inscribed in PANDA fiber showing slow and fast peaks.

By applying a double normalization to the sensitivity matrix, the system's conditioning was drastically improved, reducing the condition number to as low as 1.76. ML models, particularly Random Forest, further enhanced prediction accuracy, achieving a Root Mean Square Error (RMSE) of $0.33°C$ and $95.75\,\mu\epsilon$.

This article is structured into four main sections. The **Introduction** presents the problem and summarizes previous research efforts in the field. The **Materials and Methods** section describes the optical fibers analyzed, as well as the signal processing. In the **Results** section, the outcomes obtained through the analytical and machine learning strategies are presented. Finally, the **Discussion** section provides a critical analysis of the performance of the most effective approaches. The paper concludes with a summary of the key findings and a discussion of possible future developments.

MATERIALS AND METHODS

PANDA PM optical fibers (Figure 1) are designed to maintain light polarization by introducing birefringence through stress-applying parts (SAPs) in the cladding. This structure creates fast and slow axes with distinct refractive indices, leading to two Bragg reflection peaks when an FBG sensor is inscribed. These peaks respond differently to strain and temperature, enabling dual-parameter sensing.

The sensor analyzed exhibited Bragg peaks at $1549.80\,nm$ and $1550.14\,nm$ and was calibrated over a broad temperature range ($-10\,°C$ to $100\,°C$) and strain levels up to $8000\,\mu\epsilon$. The inverse problem was solved considering the fast peak and peak separation. Combined tests were carried out by varying the strain while keeping the temperature constant and vice versa. The effectiveness of the proposed approach was also verified, at $-5\,°C$ with varying strain, by considering five systems: (i) fast and slow peaks, (ii) fast peak and the peak separation, (iii) slow peak and the peak separation, (iv) fast peak, slow peak, and their separation and (v) mean of the peaks and peak separation.

After evaluating the system's performance, its stability with respect to input data perturbations was analyzed. The system showed an high condition number ($K = 2282957.8$), highlighting strong sensitivity to measurement noise and potential numerical instability. To address this, both analytical strategies and algorithmic approaches avoiding explicit

matrix inversion, such as ML methods, were explored. Singular Value Decomposition (SVD) was used to investigate the ill-conditioning, and the inverse solution was tested by perturbing the input vector along the direction of maximum singular value. Despite this being the best-conditioned direction, significant deviations in estimated strain and temperature confirmed the inverse problem's ill-posed nature. Conditioning strategies included matrix rescaling, evaluated through condition numbers, stability and consistency of solutions. Further stabilization techniques, such as singular value truncation, Tikhonov regularization and hybrid regularization with diagonal adjustment, were also considered.

To estimate strain and temperature from the sensor without inverting the calibration matrix, a supervised ML approach was adopted. The dataset combined measurements from thermal and mechanical calibration and one of the mixed-condition tests. Input features included the wavelength of the fast and slow peaks and their difference, while target outputs were independently measured strain and temperature. Data, 395400 samples, were split into training and testing sets using an 80 % - 20 % hold-out strategy.

Three models were implemented: Random Forest Regression (RF), Multiple Linear Regression (LR) and Artificial Neural Networks (ANNs). The Random Forest used 100 trees with out-of-bag validation, identifying feature importance. This ensemble method was chosen due to its ability to handle non-linear relationships and to provide robust predictions even in the presence of noisy measurements. An analysis of the correlation between the optical features and the target variables revealed a strong linear dependence, thus justifying the use of a multiple Linear Regression model to establish a simple and interpretable baseline for comparison with more complex approaches.

Finally, an ANN was implemented, composed of two hidden layers with 128 and 64 neurons, respectively. Each hidden layer employed the ReLU activation function, followed by batch normalization and dropout regularization with a dropout rate of 30 %. The network for strain and temperature predictions was trained using the Adam optimization algorithm, with a learning rate set to 0.001, over 50 epochs and with a mini-batch size of 512. Input and output variables were normalized using min-max scaling to enhance stability and convergence during the training phase.

RESULTS

The calibration results indicate that the wavelengths of both peaks increase with temperature, while their spectral separation decreases. This behavior yields sensitivity coefficients with opposite signs for the individual peaks and their relative spacing. For the mechanical sensitivity, both peak wavelengths exhibit a positive shift with increasing strain applied to the fiber, accompanied by an increase in the spectral separation between the two peaks. The extracted sensitivity coefficients are reported in Table II. The sensor performance was evaluated in response to variations in strain or temperature (Figure 2).

The residuals between the actual and calculated variables were evaluated, resulting in a distribution with a mean and standard deviation of $6.75 \pm 8.44\,^{\circ}C$ and $62.99 \pm 66.19\,\mu\epsilon$. To assess the improvement in accuracy by tracking only the fast peak and its separation from the slow one, all possible combinations for the resolutive system were evaluated. The comparison, conducted at $-5\,^{\circ}C$ with varying strain, is reported in Table III.

To improve matrix stability and reduce its condition number, singular values were

TABLE II. Thermal and mechanical sensitivity of fast peak, slow peak and peak separation.

	$K_T\,[nm/°C]$	$K_\epsilon\,[nm/\epsilon]$
Fast Peak	0.0113	1263.87
Slow Peak	0.0108	1273.42
Peak Difference	-0.0005	9.6483

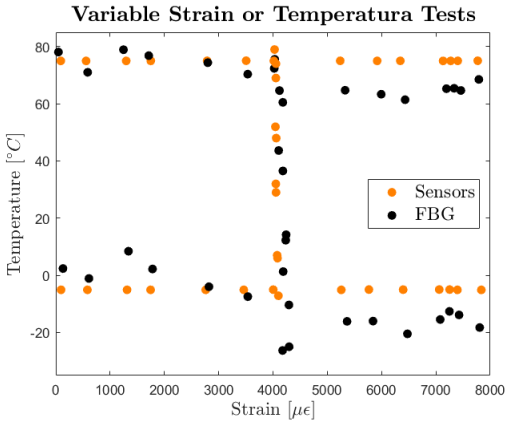

Figure 2. Numerical results and experimental measurements: two tests at constant temperature varying strain and one test at constant strain varying temperature.

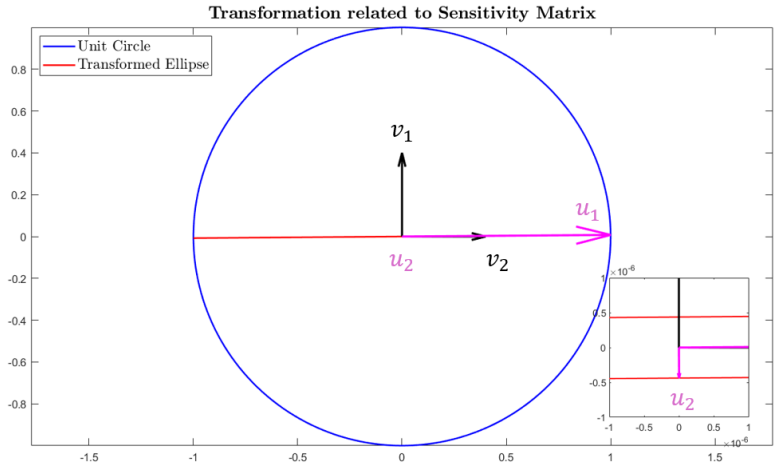

Figure 3. Right and left singular vectors of transformation associated with matrix K and effect of transformation on a unit circle.

computed, revealing principal transformation directions. The singular values obtained were $\sigma_1 = 1263.91$ and $\sigma_2 = 0.00055$. Figure 3 illustrates the directions of both the left and right singular vectors (u_1,u_2 and v_1,v_2), as well as the effect of the transformation, which maps the unit circle into a highly flattened ellipse. The ellipse is plotted using normalized dimensions to ensure clarity of the visualization.

Considering the principal directions, the system's response was analyzed under a small input perturbation of magnitude 10^{-6}. Among various scaling strategies, the most effective involved first normalizing each column by its 2-norm, followed by row-wise

TABLE III. Residuals between measured and calculated variables. Fast peak, slow peak and their separation (FSD). Fast and slow peaks (FS). Fast peak and peak separation (FD). Slow peak and peak separation (SD). Mean of peaks and peak separation (MD).

	FSD	**FS**	**FD**	**SD**	**MD**
$\mu_{residual}(\Delta T)\,[^{\circ}C]$	5.14	5.75	4.85	4.84	4.84
$\mu_{residual}(\epsilon)\,[\mu\epsilon]$	-53.21	-58.48	-50.44	-50.78	-50.60

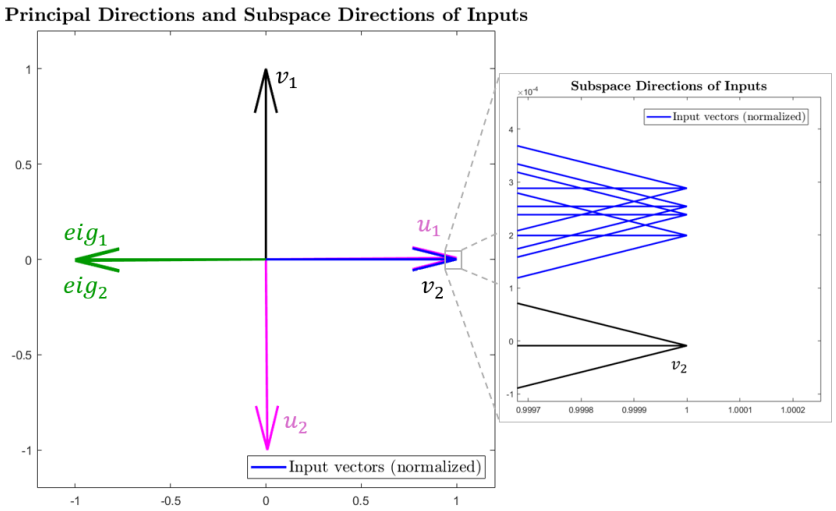

Figure 4. Directions of right and left singular vectors, directions of eigenvectors and directions of vectors defining the subspace of possible inputs.

2-norm normalization. This reduced the condition number from 1151158 to 1.76, and the error amplification from 1151010 to 1.61, with a modest change in determinant (from 0.985 to 0.859). In contrast, using the commonly adopted sensitivity matrix (in $pm/^{\circ}C$ and $pm/\mu\epsilon$) resulted in a higher condition number (139.76) and error amplification (21.35). Although other strategies were identified that could further reduce the condition number, these modifications excessively altered the system, preventing the correct capture of its physical solutions. Analysis of the input subspace (Figure 4) revealed that the input vectors are approximately aligned with the eigenvectors, indicating that the transformation predominantly scales the inputs with minimal rotational effect. Consequently, within the expected range of input variations, the system can be considered stable regardless of the specific column scaling applied.

After processing the calibration matrix, the ML models, namely the ANN, RF and LR were evaluated. The predicted and measured strain and temperature for RF model are presented in Figure 5, while the RMSE of the residuals is reported in Table IV.

TABLE IV. Root Mean Square Error of solution strategies. K sensitivity matrix; ANN (Artificial Neural Network), LR (Linear Regression) and RF (Random Forest).

	Matrix K	**ANN**	**LR**	**RF**
$RMSE_{strain}[\mu\epsilon]$	132.12	147.66	130.22	95.75
$RMSE_{temperature}[^{\circ}C]$	8.26	2.51	7.77	0.33

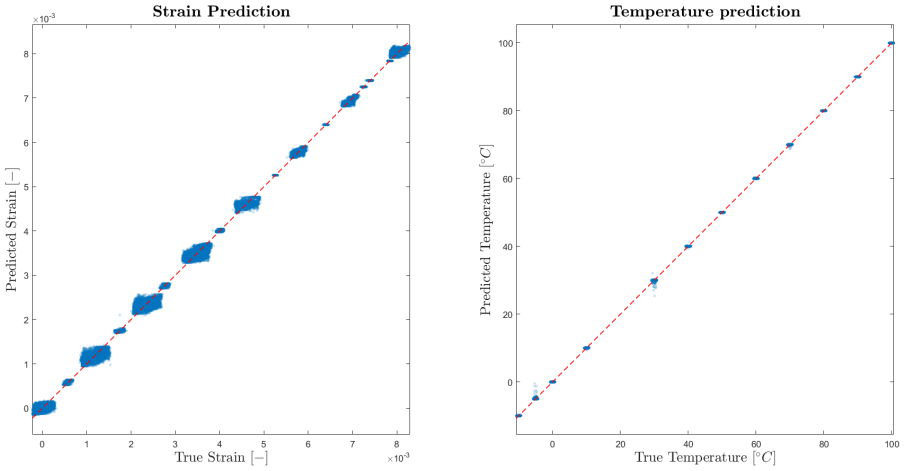

Figure 5. Predicted and true values of strain and temperature from Random Forest model.

DISCUSSION AND COMPARISON

The use of FBG sensors inscribed in PM optical fibers has demonstrated the capability to decouple thermal and mechanical effects, offering a compact and robust sensing approach. Among the evaluated resolution strategies, the combined use of the fast peak and peak separation yielded superior performance, effectively reducing residuals and enhancing the numerical conditioning of the system.

The principal directions identified through SVD analysis revealed that the transformation significantly stretches the input data along a dominant axis, underscoring the ill-posed nature of the inversion problem. A double normalization strategy, based on sequential rescaling of the system matrix using the 2-norm, first by column and subsequently by row, substantially improved the system's numerical stability. This approach reduced the condition number from values exceeding one million to approximately 1.76, effectively minimizing error amplification while preserving the determinant. Although alternative scaling strategies were investigated, they introduced excessive distortion to the system's physical response, thereby compromising the accuracy of the results. Furthermore, the identification of the subspace of feasible inputs confirmed that the system maintains adequate stability even in the absence of matrix rescaling.

Furthermore, machine learning techniques, particularly RF regression, outperformed traditional analytical inversion methods in terms of prediction accuracy, achieving RMSE values as low as $0.33\,^{\circ}C$ for temperature and $95.75\,\mu\epsilon$ for strain. Out-of-bag error analysis facilitated the identification of the most influential input parameters among the three considered (fast peak, slow peak, and peak separation). Strain prediction was influenced by the fast axis response, while temperature estimation was more strongly correlated with the peak separation. Although LR models exhibited lower predictive performance overall, they demonstrated better generalization capabilities on previously unseen datasets. This observation underscores the importance of further validating the system with new data.

CONCLUSIONS AND FUTURE DEVELOPMENTS

This study demonstrated that PM optical fibers inscribed with FBG sensors constitute an effective solution for thermo-mechanical decoupling in aerospace applications and SHM. The proposed analytical enhancements led to an improvement in system robustness, as evidenced by the substantial reduction in the condition number and associated error amplification. Furthermore, machine learning techniques, particularly Random Forest regression, outperformed conventional strategies, maintaining high prediction accuracy even under conditions of measurement noise. Future research will focus on optimizing the integration of these sensors within composite structures to ensure minimal interference and enhanced performance. Additionally, the stability of the system matrix will be analyzed with respect to its coefficients. Based on this analysis, the data acquisition cycle may be modified accordingly to improve sensor calibration and overall system reliability.

ACKNOWLEDGMENT

This research has been supported by ASI (Italian Space Agency), grant agreement 2018-5-HH.0.

REFERENCES

1. Zhou, Z. and J. Ou. 2005. "Techniques of Temperature Compensation for FBG Strain Sensors Used in Long-Term Structural Monitoring," in *Fundamental Problems of Optoelectronics and Microelectronics II*, vol. 5851, pp. 167–172.
2. Hu, Q., P. Wang, B. Rao, M. Wang, Z. Wang, and X. Xu. 2020. "Simultaneous measurement of temperature and strain using double-cladding fiber based hybrid Bragg grating," *OSA Continuum*, 3(4):1031–1037, doi:10.1364/OSAC.389645.
3. Jiang, Y., C. Liu, W. Zhang, D. Mao, D. Yang, and J. Zhao. 2017. "Multi-Parameter Sensing Using a Fiber Bragg Grating Inscribed in Dual-Mode Fiber," *IEEE Photonics Technology Letters*, PP:1–1, doi:10.1109/LPT.2017.2737013.
4. Triollet, S., L. Robert, E. Marin, and Y. Ouerdane. 2011. "Discriminated measures of strain and temperature in metallic specimen with embedded superimposed long and short fibre Bragg gratings," *Measurement Science and Technology*, 22(1):015202, doi:10.1088/0957-0233/22/1/015202.
5. Hopf, B., B. Fischer, T. Bosselmann, A. W. Koch, and J. Roths. 2019. "Strain-Independent Temperature Measurements with Surface-Glued Polarization-Maintaining Fiber Bragg Grating Sensor Elements," *Sensors*, 19(1):144, ISSN 1424-8220, doi:10.3390/s19010144.
6. Casciaro, E., T. Scalia, M. Albano, and P. Bettini. 2024. "SHM of Space Structures: Use of Polarization-Maintaining Fibers to Decouple the Thermo-Mechanical Effect on Fiber Bragg Grating Sensor Measurements," in *75th International Astronautical Congress (IAC)*, International Astronautical Federation (IAF), Milan, Italy, doi:http://dx.doi.org/10.52202/078369-0169.
7. Casciaro, E., D. Rigamonti, and P. Bettini. 2024. "Birefringent Optical Fibers to Decouple Thermo-Mechanical Effects on FBG Sensors," in *11th European Workshop on Structural Health Monitoring (EWSHM)*, EWSHM, Salzburg, Austria, doi: http://dx.doi.org/10.58286/29849.